ISSN: 2755-0125

Journal of Virology Research & Reports

SCIENTIFIC Research and Community

Research Article

Open Access

# Alterations in Lung Carcinoma Cells and Cell-Derived Extracellular Vesicles after Human Adenovirus Type 5 Administration

**Brennetta J Crenshaw[1], Ayodeji O Ipinmoroti[1], Rachana Pandit[1], Brian Sims[2], Sameer Joshi[3] and Qiana L Matthews[1,4*]**

[1]Microbiology Program, Department of Biological Sciences, College of Science, Technology, Engineering, and Mathematics, Alabama State University, Montgomery, USA

[2]Departments of Pediatrics and Cell, Developmental and Integrative Biology, Division of Neonatology, University of Alabama at Birmingham, Birmingham, USA

[3]Department of Pharmaceutical Sciences, College of Pharmacy, Larkin University, Miami, USA

[4]Department of Biological Sciences, College of Science, Technology, Engineering, and Mathematics, Alabama State University, Montgomery, USA

**ABSTRACT**

Human adenoviruses (HAdVs) affect the respiratory system of healthy individuals and people with pre-existing health conditions. These highly infectious viruses can alter a myriad of cellular and pathophysiological processes. HAdVs can modulate their infection ability and pathogenicity by regulating extracellular vesicles (EVs) formation and function. EVs are nanovesicles that facilitate intracellular communication, cell signaling/trafficking, and immune regulation. We propose that HAdVs can exploit EV formation, secretion, and release various pathways to promote infection and transmission between neighboring cells. In the present study, we explored the impact of HAdV serotype 5 (HAdV-5) on the A549-epithelial carcinoma cells and EVs derived from A549 cells. A549 cells were cultured in an exosome-depleted medium and administered different concentrations of HAdV-5 at varying time points. The effect of HAdV-5 infection on A549 cells and A549-derived EVs was determined by 4',6-diamidino2-phenylindole (DAPI) stain, 3-(4, 5-dimethylthiazol-2-yl)-2, 5-diphenyl tetrazolium bromide (MTT) assay, electron microscopy, particle size, zeta potential analysis, immunosorbent analysis, total RNA levels, and total protein content. Our findings illustrated that HAdV-5 reduces A549-cell viability and promotes variations within the protein content of A549 cells. Our data explicitly demonstrated that HAdV-5 significantly altered EV numbers, biogenesis, and composition. These findings suggest that HAdV-5 modulates EVs' biological properties and physiological functions in human lung carcinoma cells.

***Corresponding author**

Qiana L Matthews, Department of Biological Sciences, College of Science, Technology, Engineering, and Mathematics, Alabama State University, Montgomery, AL 36104, USA. Tel: 334-604-8443.

**Received:** July 20, 2023; **Accepted:** July 21, 2023; **Published:** July 31, 2023

**Keywords:** Adenovirus, Extracellular Vesicles, Exosomes, Apoptotic Bodies

## Introduction

Human adenoviruses (HAdVs) are a family of non-enveloped DNA viruses [1, 2]. They spread from an infected person through personal contact (e.g., touch or shaking hands), airborne droplet particles (i.e., coughing and sneezing), touching adenovirus (AdV)-contaminated surfaces (e.g., towels and doorknobs), and contaminated food and water. HAdV can cause mild-to-severe respiratory illness in immunocompromised people and occasionally in healthy individuals of all ages at any time of year. These highly contagious viruses can cause cold or flu-like symptoms. In addition, HAdV infection may lead to severe illnesses, such as pneumonia that may cause hospitalization or death [3]. According to the Centers for Disease Control and Prevention, no FDA- approved vaccines or antiviral medicines are available for AdV treatment. Most infections are mild and require the clinical care of symptoms or complications associated with the virus.

HAdV species are categorized into seven subgroups: HAdV-A to HAdV-G [1, 2]. More than 65 AdV species are reported to be pathogenic to humans [1, 4]. Varying HAdV species are associated with a multitude of illnesses, such as meningoencephalitis conjunctivitis, gastroenteritis, etc [5-10]. Specifically, group C HAdV-5 is associated with respiratory tract infections. HAdV-5 is one of the best-studied types of AdV. It is used to provide a better understanding of host cellular processes, virus biology, and virus-cell interactions during infection [11]. Clinically, HAdV-5 is used as an oncolytic agent, vaccine vector, and gene-delivery vector [12-17].Viruses frequently invade host cells through interactions of viral ligands with cell receptors. For decades, receptor-mediated virus entry has been explored in-depth [18-20]. A recent study by our group illustrated that the release of extracellular vesicles (EVs) may offer a mechanism by which HAdVs, enter cells through receptor-independent entry [21-23]. EVs are heterogeneous-sized, lipid membrane-derived vesicles secreted by prokaryotic and eukaryotic cells into the extracellular environment. There are three main types of EVs: small EVs, such as exosomes (~ 50 - 150 nm); medium-size EVs, such as microvesicles (~ 100 - 1,000

nm); and large EVs, such as apoptotic bodies (ApoBDs) (~500 - 2,000 nm). These EV subtypes are differentiated based on their origin, size, biogenesis, composition, and function. EVs facilitate intracellular communication by transporting cellular cargo (lipids, nucleic acids, and proteins) from donor to recipient cells. These vesicles have been observed in cultured medium from cells and many biological fluids (e.g., such as semen, urine, and breast milk) [2, 24-34]. EVs and viruses use similar cellular machinery to exit the cell [1, 35, 36]. Both vesicles and viruses can deliver proteins and nucleic acids to target cells. EVs released from viral-infected cells play a significant role during the progression of virus infections. They carry viral genomes and act as cargo for viruses, which is essential for viruses to invade, spread, survive within the host, and infect the host [35-37]. In the proposed study, we investigated the impact of HAdV-5 on lung carcinoma cellular biology and lung carcinoma-derived EV biogenesis and composition. We hypothesize that EVs are released in the media of HAdV-5-infected lung carcinoma cells. These vesicles will release genetic constituents and viral proteins that aid in cell-to-cell communication and immune modulation between neighboring cells. This study will increase our understanding of the complex relationship between viruses and EVs.

## Materials and Methods

### Cell Culture and Virus Infection

Human lung carcinoma cell line A549 was purchased from American Type Culture Collection (Manassas, VA, USA). A549 cells were cultured in Dulbecco's Modified Eagle Medium/Nutrient Mixture F-12 (DMEM/F-12) containing 1X L-glutamine supplemented with 10% Corning Regular Fetal Bovine Serum (FBS), 1% penicillin/streptomycin, and 0.2% Amphotericin-B (0.5 µg/mL) (all from Fisher Scientific; Grand Island, NY, USA) at 37°C, in a 5% $CO_2$ incubator. The cells were grown to 70-80% confluency before proceeding with experiments. For virus and EV experiments, A549 cells were plated in 60 mm cell culture dishes at a density of $5\times10^5$ cells/dish and incubated at 37°C and 5% $CO_2$ incubator overnight before HAdV- 5 administration. For virus infection, the media was removed from each dish and replaced with either exosome-free DMEM/F-12 media containing 2% exosome-depleted FBS (System Biosciences; Palo Alto, CA, USA) only (control) or exosome-free DMEM/F-12 media containing dilutions of HAdV- 5 ($2 \times 10^9$ vp/µL) at 300, 750, and 1500 multiplicity of infection (MOI). The infection duration was 24 hours (h) or 72 h. All experiments were performed using four to six independent replicates.

### Fluorescence Imaging

A549 cells were subjected to DAPI fluorescence to visualize the nuclei of cells after virus exposure at 24 h or 72 h. In brief, $1\times10^5$ cells/well were plated in a 6-well tissue culture plate and administered a range of HAdV-5 concentrations. Post-virus infection, the cells were washed with 1X phosphate buffered saline (PBS) (1-3 times) and stained with 300 nM DAPI stain solution (Fisher Scientific; Grand Island, NY, USA). The plate was incubated for 5-10 min at room temperature (RT). Following incubation, the cells were washed again with 1X PBS (1-3 times). Images were captured using the DAPI channel on an EVOS FLc digital inverted microscope (Thermo Fisher Scientific; Waltham, MA, USA).

### Cellular Lysis

A549 cells were lysed to extract proteins from cultured cells infected with HAdV-5. Post-incubation, the cell culture medium was removed from the culture dish, and the cells were washed with 1 mL of 1X PBS. Approximately 400 µL/60 mm culture dish of 1X cell culture lysis buffer (Promega; Madison, WI, USA) containing 1X protease inhibitor (Thermo Fisher Scientific; Waltham, MA, USA) was added to the cells per dish. The cells were gently scraped from the dish using a cell scraper and centrifuged at 12,000 × gravity (g) for 15 seconds (sec) at RT, using an Eppendorf 5415C Centrifuge (Eppendorf; Framingham, MA, USA). The supernatant was collected and stored at −80 ◦C until further use.

### Cell Viability Assay

A549 cell viability was assessed using the MTT assay (Thermo Fisher Scientific; Waltham, MA, USA). The cells ($1\times10^4$ cells/well) were seeded in a 96-well tissue culture plate and maintained in culture overnight prior to infection. The next day, the culture media was replaced with exosome-free media; and the cells were infected with HAdV-5 at varying concentrations, previously mentioned, for 24 h or 72 h. Post-infection, the cells were administered 50 µL of 5 mg/mL MTT/1X PBS and incubated for 4 h at 37 °C in a 5% $CO_2$ incubator. Following incubation, 100 µL of dimethyl sulfoxide was added to each well. Absorbance was read at 590 nm using the BioTek Synergy HTX multi-mode reader (Agilent; Santa Clara, CA, USA). All samples were evaluated in triplicate.

### EV Isolation and Purification

EVs were isolated from the supernatant of non-infected (control) or HAdV-5-infected cells using a combination of centrifugation and filtration. The vesicles were purified via ultracentrifugation. The media was collected post-infection and centrifuged at 300 × g for 10 min at 4°C, using a Sorvall RT 6000 centrifuge (Sorvall; Ontario, Canada, USA). For large EV (i.e., apoptotic bodies) isolation, the supernatant was collected and centrifuged again at 3,000 × g for 20 min at 4°C, followed by filtration using a 5.00 µm filter to obtain large vesicles. For small EV (i.e., exosomes) isolation, the supernatant was collected and filtered through a 3 mL syringe with a 0.22-µm filter to remove large particles. The exosomes were then subjected to 1X PBS containing 5% sucrose and 1X protease inhibitor and centrifuged at 110,000 × g for 70 min at 4 °C in a SW41Ti swinging bucket rotor using a Beckman Coulter Optima ™ L-70 K Ultracentrifuge (Beckman Coulter; Brea, CA, USA). After ultracentrifugation, the media was decanted. Approximately (~) 500 µL of EV pellets were collected from each sample and stored at − 20°C.

### Extraction of Exosomal RNA

RNA was extracted from EVs using the TRIzol method (Invitrogen; Waltham, MA, USA). 5 µg of EV samples were subjected to 5% sucrose (Fisher Scientific; Grand Island, NY, USA) and 1% Triton rX -100 (Thermo Fisher Scientific; Waltham, MA, USA) and incubated on ice for 30 min. Following incubation, the samples were treated with micrococcal nuclease (Thermo Fisher Scientific; Waltham, MA, USA), 1 MTris hydrochloride (pH 8.0) (Fisher Scientific; Grand Island, NY, USA), and 100 mM Calcium chloride (Thermo Scientific; Waltham, MA, USA) and boiled at 37°C for 15 min. Next, RNA was isolated from the EVs using the TRIzol extraction method according to the manufacturer's procedures [38]. Total levels of RNA in EVs were quantified using NanoDrop One (Thermo Fisher Scientific; Waltham, MA, USA) and stored at −80 C until further use.

### Total Protein Quantitation

Total protein content of A549 lysates or A549-derived EVs were quantitated using a Bicinchoninic acid (BCA) assay (Bio-Rad Laboratories; Hercules, CA, USA). 5 µL of bovine serum albumin (BSA) standards (0, 0.2, 0.4, 0.8, and 1.6 µg/µL), A549 lysates, or EV samples were plated in a 96-well microtiter plate. Next, reagent

A (25 µL) and reagent B (200 µL) were added to each well. The plate was wrapped in aluminum foil and placed on a shaker at low speed for 15 min. Absorbance was measured at 630 nm using a BioTek Synergy LX Multimode Reader (Fisher Scientific; Grand Island, NY, USA). A standard curve was prepared to determine the total protein concentration in cell lysates or EVs. Samples were evaluated in triplicates.

**Particle Tracking Analysis of Exosomes**

Exosome size distribution and concentration (particle/mL) were analyzed using Zeta View nanoparticle tracking analysis (NTA) (NanoSight-LM10, Malvern Instruments, Inc., Malvern, UK) according to the manufacturer's instructions. NTA analyzes exosome particle size and concentration based on the Brownian particle movement and light scattering. In brief, exosome samples were diluted at 1:100 in sterile 1 × PBS and loaded into a 0.3 mL disposable syringe. Five independent analyses were evaluated. The mean values were calculated to determine exosome size.

**Scanning Electron Microscopy**

The size and structure of ApoBDs were visualized by scanning electron microscopy (SEM). ApoBDs were fixed in 2% glutaraldehyde after isolation. The samples were placed on carbon tape, mounted on a stud, and dried overnight under a ventilation hood. Prior to imaging, a coating of 2-5 nm gold-palladium alloy was applied by sputtering. The samples were imaged using a JEOL JSM-7600F SEM (Center for NanoBiotechnology Research: Alabama State University; Montgomery, AL). SEM was performed under low beam energies (5.0-10.0 kV).

**Transmission Electron Microscopy**

Exosome size and morphology were evaluated using transmission electron microscopy (TEM) [2, 25, 28]. For sample preparation, exosome samples were suspended in 1X PBS containing 5% glutaraldehyde, loaded on the EM grid, and incubated at RT for 1 min. The exosomes were immediately stained with 7 µL of filtered uranyl acetate solution on the surface of the EM grid. After 15 secs, the solution was removed, and the samples were observed under TEM Tecnai 120 kV (FEI; Hillsboro, OR, USA) at 80 kV within 24 h as compared to the negatively stained grids. Digital images were captured with a BioSprint 29 CCD Camera (AMT; Woburn, MA, USA).

**Zeta Potential Analysis**

The surface charge of EVs was determined by zeta potential (ZP) analysis using a Zetasizer Nano ZS system (Malvern Instruments, Malvern, UK). ZP is calculated by determining electrophoretic mobility in suspension using dynamic light scattering. For ZP measurements, 10 µL of EV aliquots were diluted in 990 µL of deoxidized water and then transferred to a Malvern Clear ZP cell. Three to five independent EV aliquots were analyzed. Three measurements were taken for each aliquot. The data was analyzed using the Zeta Sizer Software.

**Western and Dot Blot Analysis**

The expression of EV-associated proteins/markers was evaluated by western and/or dot blot analysis. For western blot, 30 µg of EV samples were utilized and 5µg of A549 lysates or EV proteins were subjected to 5X lane maker reducing sample buffer (1:1 ratio) and boiled at 99˚C for 10 min. For western blot analysis, the EV samples were loaded in a 10% 1.5 mm precast gel (BioRad) and ran at 100 V for 1 h. The proteins were transferred onto polyvinylidene difluoride (PVDF) membranes at 45 mA overnight. For dot blot analysis, either the A549 lysates or EV proteins were blotted on nitrocellulose membranes and dried for 5-10 min at RT. The membranes were blocked for non-specific binding with 5% nonfat dry milk for 30 min at RT on a shaker.

After blocking, the membranes were subjected to specific primary antibodies against the following proteins: B cell lymphoma (BCL)-2 (1:500 dilution), Heat shock protein (Hsp) 27 (1:500 dilution), Hsp 60 (1:250 dilution), Hsp 100 (1:250 dilution), Histone deacetylase (HAD) 3 (1:500 dilution) (all from DSHB; Iowa City, IA, USA), Hsp 70 (1:500 dilution), Hsp 90β (1:75 dilution), Annexin V (1:500 dilution), Rab 35 (1:500 dilution), Interleukin (IL) 12 (1:500 dilution), and Toll-like Receptor (TLR) 6 (1:500 dilution) (all from Invitrogen: Thermo Fisher Scientific; Waltham, MA, USA) overnight with gentle shaking at 4°C. The next day, the membranes were washed with 1 × Tris-buffer-saline (TBS) buffer containing 0.08% Tween-20 (TBST-20) three times for 10 min each. Following washing, the membranes were incubated with the appropriate horseradish peroxidase-conjugated secondary antibodies: Goat anti-mouse IgG (H+L), Horseradish peroxidase (HRP) (Promega; Madison, WI, USA, 1: 2,000 dilution) or goat anti-rabbit IgG (H+L) HRP (Thermo Fisher Scientific; Waltham, MA, USA, 1: 2,000 dilution) on a shaker for at RT 1 h. The blots were washed with 0.08% Tween-20 in 1 × PBS three times for 10 min each. The nitrocellulose membranes were developed using Super Signal West Femto Maximum Sensitivity Substrate (Thermo Scientific, Waltham, MA, USA). The signals were read on a Bio-Rad ChemiDoc XRS + System (Bio-Rad Laboratories; Hercules, CA, USA) using chemiluminescence.

**Statistical Analysis**

Statistical analyses were performed with the Graph Pad Prism 5 (San Diego, CA, USA) software using a one-way ANOVA with Tukey post hoc analyses. The Tukey multiple- comparison tests performed are defined as the following: *$P \leq 0.05$, **$P \leq 0.01$, and ***$P \leq 0.0001$. Data are displayed as mean ± standard deviation or standard error (as indicated).

## Results

**Human Adenovirus Type 5 Exposure Reduces A549 Cell Viability**

A549 cells were exposed to exosome-depleted DMEM/F12 media containing dilutions of HAdV-5 at MOI 300, MOI 750, and MOI 1500 vp/cell for 24 h or 72 h. Post-infection, cell viability was assessed using fluorescence microscopy and the MTT assay to investigate the impact of HAdV-5 on A549 cells. DAPI stain was used to visualize the nucleus of cells after HAdV-5 infection. DAPI binds to and 'stains' double- stranded DNA within live or fixed cells. We observed vibrant blue fluorescence in the A549 cells among all experimental groups at both 24 h (Figure 1A) and 72 h time-points (data not shown). Cell viability was accessed via MTT assay. At 24 h post-infection (hpi), our findings demonstrated that A549 cell viability was significantly reduced by 10% in cells at MOI 750 vp/cell and by 11% at the highest virus concentration (MOI 1500 vp/cell) when compared to noninfected virus cells (control) ($P \leq 0.05$; Figure 1B). At 72 h HAdV-5 administration, A549 cell viability decreased significantly among all experimental groups: 25% at MOI 300 vp/cell, 25% at MOI 750 vp/cell, and 15% at MOI 15 00 vp/cell compared to the control group ($P \leq 0.05$ and $P \leq 0.001$; Figure 1C). Our results showed that HAdV-5 exposure reduced A549 cell viability dose- dependently.

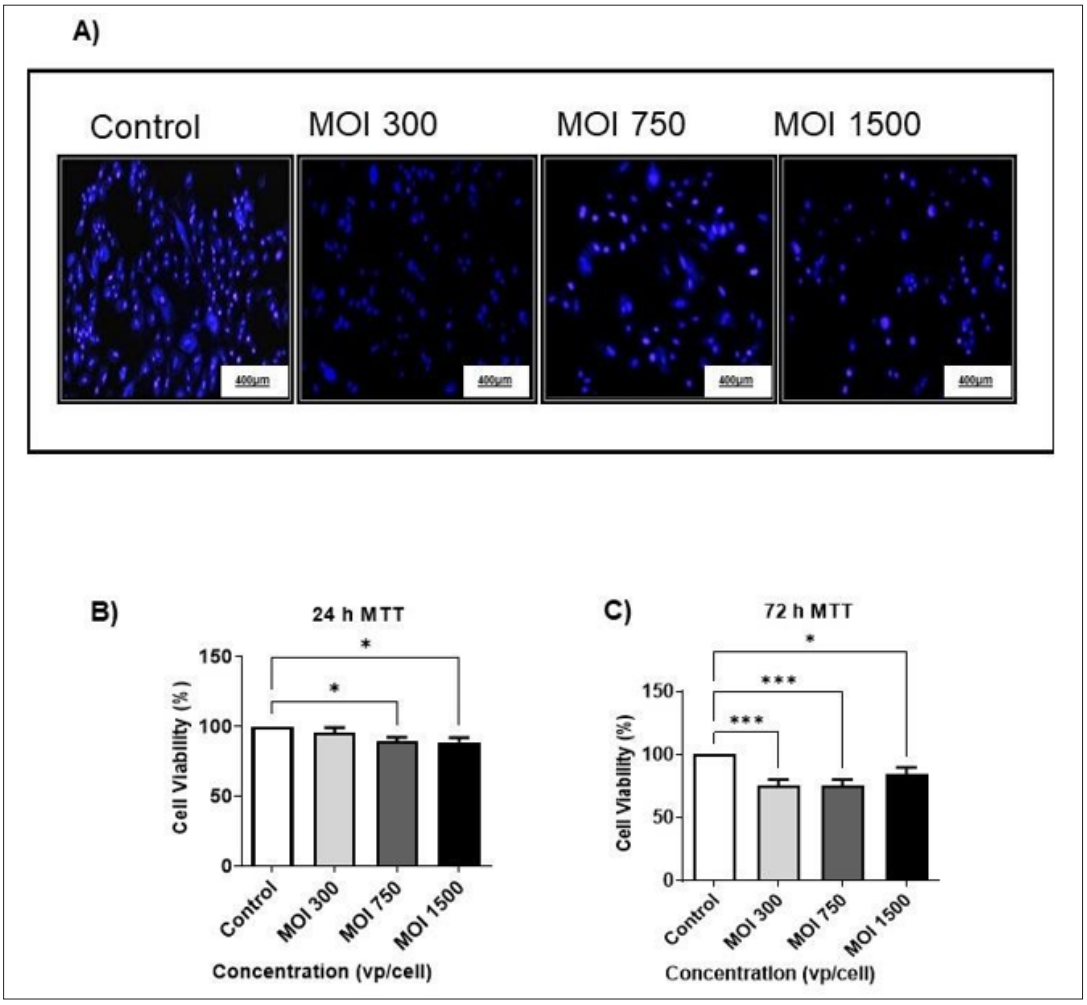


**Figure 1: Impact of Human Adenovirus Type 5 on Lung Carcinoma Cells**

A549 cells were administered HAdV-5 at MOI 300, MOI 750, and MOI 1500 vp/cell. (A) DAPI stain of A549 cells after 24 h HAdV-5 exposure. DAPI is a fluorescent stain used to visualize the membrane permeability of dead cells. Under fluorescence microscopy, the dead cells fluoresce blue. The images were captured on an EVOS digital inverted microscope using the DAPI channel, 10X magnification, 400 µm scale. Cell viability was assessed by the MTT assay at (B) 24 h and (C) 72 hpi. Statistical significance was obtained from five independent experiments in triplicates and determined using one-way ANOVA with post hoc Tukey's analysis. Data are presented as the mean ± SEM as follows: (*) $P \leq 0.05$ and (***) $P \leq 0.001$.

**HAdV-5 Alters Stress Response in Lung Carcinoma Cells**

A549 cells were subject to HAdV-5 at varying concentrations for 24 h or 72 h. A549 cells were lysed as previously described. The protein concentration of A549 cell lysate was quantified using a BCA assay. Dot blot analysis was performed to examine the expression of Hsps in A549 lysates after 24 h or 72 h viral administration (Figures 2A-E). Hsps are a large family of molecular chaperones produced by cells in response to stressful stimuli (e.g., bacteria and viruses) [39-42]. They regulate and facilitate protein folding and unfolding, assembly and disassembly, translocation, degradation, cell survival, etc. Some Hsps can have an antiviral effect during viral infection by inhibiting viral proliferation. These chaperones interact with virus-associated molecules and initiate immune signaling pathways to protect the host cell . Hsps are often hijacked by viruses. Viruses utilize Hsps to help them invade, replicate, mature, and survive inside the host cell [42]. We first evaluated Hsp 27, a small regulatory Hsp (Figure 2A). At 24 h post-virus infection, we observed no significant change in Hsp 27 expression levels in lysates (Figure 2A). However, at 72 h virus exposure, we found that Hsp 27 expression in A549 cell lysates was significantly elevated among all experimental groups (MOI 300, MOI 750, and MOI 1500 vp/cell) compared to control lysates when cells were infected with HAdV-5 ($P \leq 0.001$, $P \leq 0.01$, and $P \leq 0.0001$; Figure 2A). Furthermore, we observed significantly high levels of Hsp 27 expression in cell lysates at MOI 750 vp/cell and MOI 1500 vp/cell ($P \leq 0.01$; Figure 2A). Next, we examined Hsp 60, a well-studied molecular chaperone (Figure 2B). Cells infected with HAdV-5 at 24 h exhibited a significant increase in expression of Hsp 60 from uninfected lysates (control) to infected lysates at MOI 750 vp/cell ($P \leq 0.05$; Figure 2B). In addition, the expression of Hsp 60 was significantly increased in A549 lysates following exposure with HAdV-5 MOI 750 vp/cell compared to lysates at HAdV-5 MOI 300 vp/cell ($P \leq 0.05$; Figure 2B). Conversely, at HAdV-5 MOI 750 vp/cell, Hsp 60 expression decreased significantly in lysates compared to cell lysates at HAdV-5 MOI 1500 vp/cell at 24 h virus administration ($P \leq 0.05$; Figure 2B). At the 72 h time-point, we observed that Hsp 60 expression in cell lysates was significantly reduced at MOI 1500 vp/cell when compared to the non-infected group (control lysates) ($P \leq 0.05$; Figure 2B). There was a significant reduction in Hsp 60 expression in lysates between the lowest HAdV-5 concentration (MOI 300 vp/cell) and the highest virus concentration (MOI 1500 vp/cell) at 72 hpi ($P \leq 0.05$; Figure 2B). Hsp 70 was also evaluated in A549

lysates at 24 h or 72 h infection (Figure 2C). Hsp 70 proteins are central components of the cellular network of molecular chaperones and protein folding and remodeling in cells. Hsp 70 was significantly reduced among all infected experimental groups (MOI 300 vp/cell; $P \leq 0.05$, MOI 750 vp/cell; $P \leq 0.05$, and MOI 1500 vp/cell; $P \leq 0.01$) compared with the control group (Figure 2C). However, at 72 h, there was no change in Hsp 70 expression between the uninfected group (control) and HAdV-5 infectious groups (Figure 2C). Hsp 90 β is the main functional protein that plays a vital role in cell viability, protein folding, degradation, and cell signaling. We observed a significant increase in levels of Hsp 90 β expression in control lysates compared to lysates at MOI 1500 vp/cell at 24 h HAdV-5 infection ($P \leq 0.05$; Figure 2D). At 72 h HAdV-5 infection, there was a slight increase in Hsp 90 β expression at MOI 300 vp/cell and MOI 750 vp/cell (Figure 2D). We further examined the effect of HAdV-5 exposure on the expression of the large molecular chaperone Hsp 100 within our A549 lysates (Figure 2E). Hsp 100 expression was significantly higher in non-infected cell lysates (control) when compared to lysates in the MOI 750 vp/ cell experimental group after 24 h HAdV-5 infection ($P \leq 0.05$; Figure 2E). However, at MOI 1500 vp/cell, we observed that Hsp 100 expression levels were reduced significantly when compared to cell lysates at MOI 750 vp/cell ($P \leq 0.05$; Figure 2E). At the 72 h time-point, Hsp 100 expression were significantly lower in A549 lysates at all three virus concentrations (MOI 300, MOI 750, and MOI 1500 vp/cell) when compared to control A549 lysates ($P \leq 0.05$, $P \leq 0.0001$, and $P \leq 0.01$; Figure 2E). Our results showed that HAdV-5 altered the stress response of stress-related proteins within the A549 lysates in a dose-dependent manner.

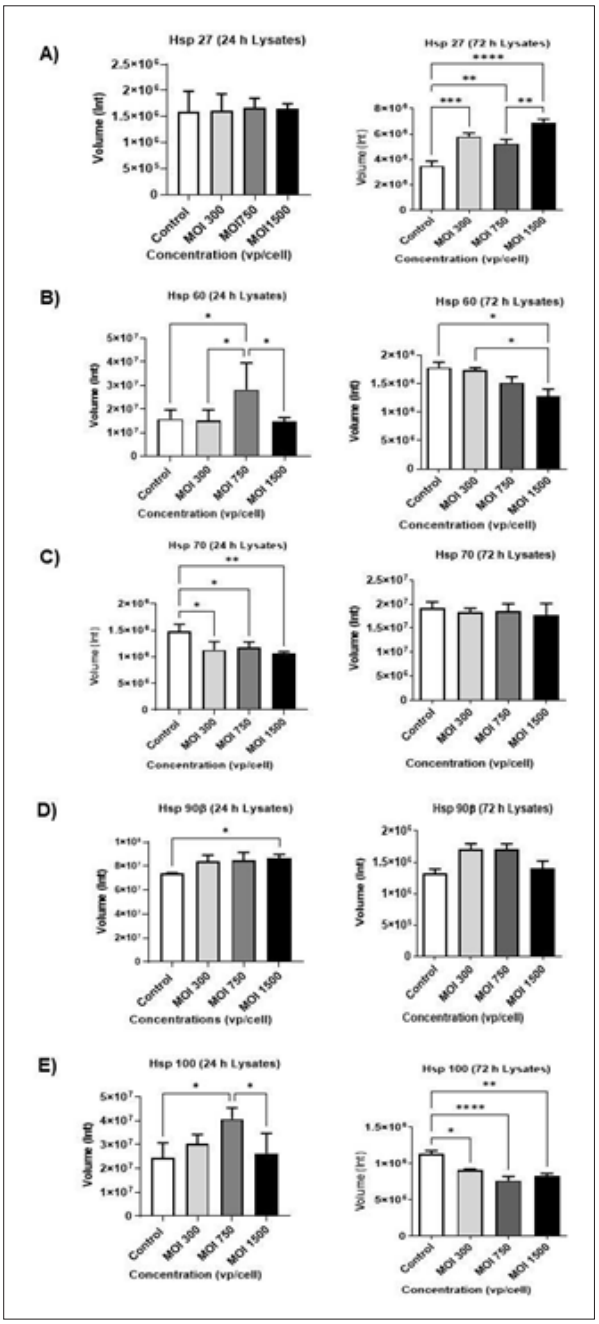


**Figure 2: Modulation of Stress Proteins in A549 Lysates**
(A) Evaluation of heat shock proteins (Hsp) 27, (B) Hsp 60, (C) Hsp 70, (D) Hsp 90β, and (E) Hsp 100 post 24 h and 72 h HAdV-5 administration. Statistical significance was obtained from five independent experiments and determined using one-way ANOVA with post hoc Tukey's analysis. Data are presented as the mean ± SEM as follows: (*) $P \leq 0.05$, (**) $P \leq 0.01$, (***) $P \leq 0.001$, and (****) $P \leq 0.0001$.

**Expression of Apoptotic-Associated Proteins in A549 Lysates**

To determine how A549 cells responded to the exposure of HAdV-5 infection, we evaluated apoptosis regulators Annexin V, BCL- 2, and HDAC 3 (Figures 3A-C). In A549 lysates, Annexin V was found to be significantly reduced at MOI 1500 vp/cell of HAdV-5 when compared to control and MOI 300 vp/cell at 24 h HAdV-5 infection ($P \leq 0.05$; Figure 3A). However, at 72 h HAdV-5 infection, Annexin V levels were significantly increased within lysates at MOI 1500 vp/cell and uninfected cells ($P \leq 0.001$), MOI 300 vp/cell and MOI 1500 vp/cell ($P \leq 0.001$), and MOI 750 vp/cell and MOI 1500 vp/cell ($P \leq 0.01$; Figure 3A). BCL-2 regulates cell death by inducing anti-apoptotic or inhibiting pro-apoptotic responses triggered by virus-infected cells [43, 44]. BCL-2 was shown to be present within A549 lysates at 24 hpi (Figure 3B). BCL-2 expression was significantly higher in A549 lysates at MOI 1500 vp/cell when compared to non-infected lysates ($P \leq 0.0001$; Figure 3B). After 72 h of infection with HAdV-5, BCL-2 levels in cell lysates were significantly increased at MOI 300 vp/cell and MOI 1500 vp/cell ($P \leq 0.001$; Figure 3B). At the 72 h time-point, BCL-2 expression in lysates increased significantly between MOI 750 vp/cell and MOI 1500 vp/cell ($P \leq 0.001$; Figure 3B). HDAC 3 regulates cellular physiological processes, such as cell proliferation, differentiation, metabolism, and innate immune response [45, 46]. In A549 lysates, HDAC 3 expression levels were significantly reduced between control group and at the highest infectious group (MOI 1500 vp/cell; ($P \leq 0.01$), MOI 300 vp/cell and MOI 1500 vp/cell ($P \leq 0.05$), and MOI 750 vp/cell and MOI 1500 vp/cell ($P \leq 0.01$) following 24 h virus infection (Figure 3C). At 72 h HAdV-5 administration, HDAC 3 levels decreased significantly in cell lysates at MOI 750 vp/cell and MOI 1500 vp/cell when compared with the control lysates ($P \leq 0.001$; Figure 3C). Furthermore, HDAC 3 expression levels were significantly reduced in our lysates at MOI 750 vp/cell when compared to lysates at MOI 300 vp/cell ($P \leq 0.01$; Figure 3C) 72 hpi. Our dot blot analysis demonstrated that the A549 cells were significantly modulated under apoptotic- related stress conditions after HAdV-5 infection.

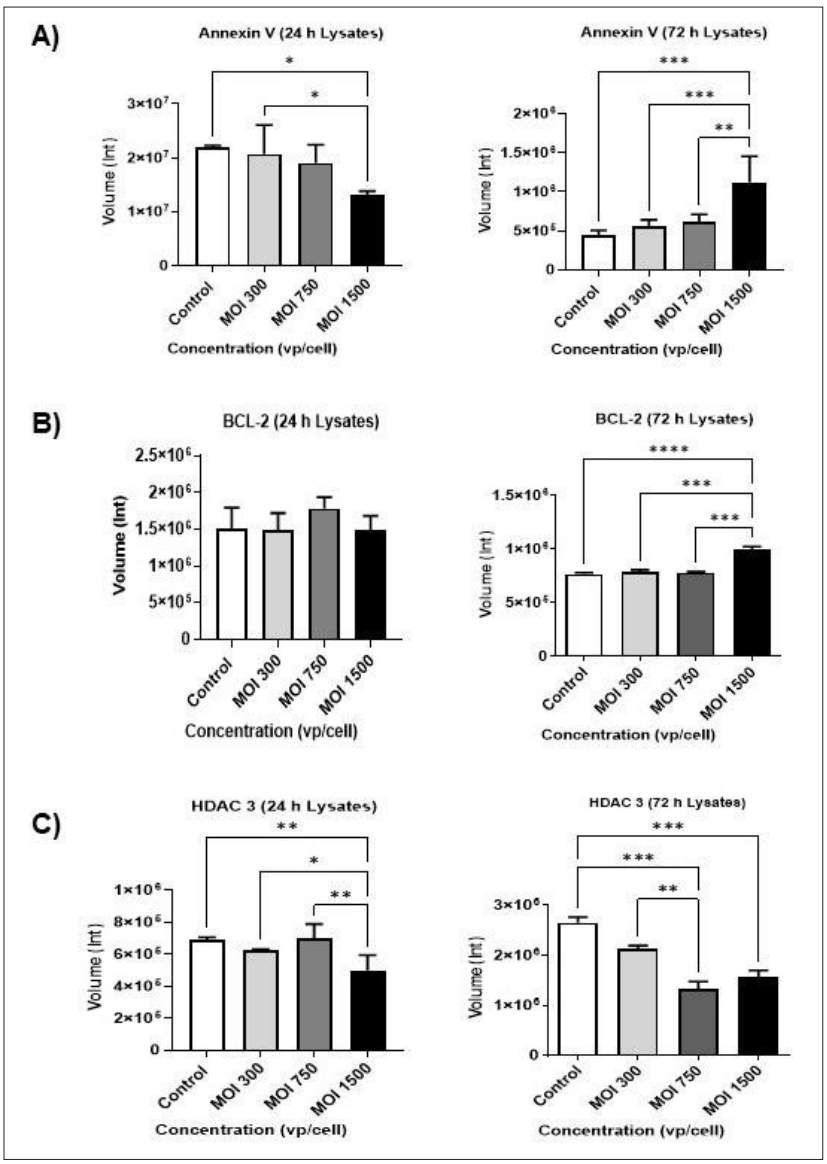


**Figure 3:** Expression of Apoptotic-Associated Proteins

Cell lysates (at 24 h and 72 h HAdV-5 administration) were evaluated for (A) Annexin V, (B) B cell lymphoma (BCL)-2, and (C) Histone deacetylase (HDAC) 3. Statistical significance was obtained from five independent experiments and determined using one-way ANOVA with post hoc Tukey's analysis. Data are presented as the mean ± SEM as follows: (*) $P \leq 0.05$, (**) $P \leq 0.01$, (***) $P \leq 0.001$, and (****) $P \leq 0.0001$.

### Characterization of A549-Derived Exosomes after Viral Infection

Purified membrane vesicles were obtained from the supernatants of non-infected and HAdV-5-infected A549 cells. They were isolated using a combination of centrifugation and filtration and purified using ultracentrifugation [2, 24-26, 28]. Exosomes are micro-sized vesicles released by cells that can be distinguished based on their morphology and size. TEM is a standard tool to visualize exosomes [47, 48]. At 24 hpi or 72 hpi, TEM data revealed that the A549 cells released a mixture of heterogeneous-sized vesicles, with diameters varying between 50-150 nm. The EVs isolated from the supernatant of uninfected A549 cells (control) and infected A549 cells at MOI 300 vp/cell were cup-shaped, spherical vesicles that contained a lipid bilayer membrane, which resembles the described characteristics for exosomes isolated from cell culture media (Figure 4A) [2, 24, 25]. NTA was utilized to validate the size distribution and concentration of the vesicles at 24 h and 72 hpi (Figures 4B-E). NTA analysis showed that the exosomes' mean size averaged < 150 nm among all vesicle groups at 24 h and 72 h post-HAdV-5 infection (Figures 4B and D). At the 72 h HAdV-5 post-infection, there was a significant increase in the mean size of small EVs (i.e., exosomes) at MOI 750 vp/cell and MOI 1500 vp/cell compared to the control vesicles ($P \leq 0.05$; Figure 4D). At 24 h and 72 h virus administration, the total number of small EVs produced at MOI 750 vp/cell and MOI 1500 vp/cell were greater than the total number of control exosomes (Figures 4C and E). Exosome surface charges were evaluated via ZP analysis (Figures 4F and I). The surface charge determines the stability of the vesicles and is known to influence different biological processes, such as cellular uptake and cytotoxicity [49, 50]. The surface potential distribution of all exosome preparations showed a negative surface charge and exhibited a ZP range of -3.16 to -34.3 mV at 24 h or 72 h viral infection (Figures 4F and I). At the 24 h time-point, the ZP values were significantly reduced in small EVs at all three virus concentrations (MOI 300, MOI 750, and MOI 1500 vp/cell) compared to non-infected (control) exosomes ($P \leq 0.001$ and $P \leq 0.0001$; Figure 4F). At 72 h HAdV-5 exposure, the ZP values decreased significantly in small EVs among all experimental groups compared to the control vesicles ($P \leq 0.05$ and $P \leq 0.0001$; Figure 4I). In addition, we observed a significant decrease in the distribution of exosomes between the lowest virus concentration (MOI 300 vp/cell) and exosomes at MOI 750 and MOI 1500 vp/cell ($P \leq 0.0001$; Figure 4I). Most importantly, we examined the RNA (Figures 4G and J) and protein levels (Figures 4H and K) within our vesicles obtained from A549 cells at 24 h or 72 h HAdV-5 infection. Figures 4G and J showed that the total RNA levels in EVs were significantly increased at all 3 virus concentrations at both time-points when compared with control EVs ($P \leq 0.01$, $P \leq 0.001$, and $P \leq 0.0001$). In addition, RNA levels in EVs were significantly greater between the lowest virus concentration (MOI 300 vp/cell) and highest virus concentration (MOI 1500 vp/cell) ($P \leq 0.0001$), as well as between EVs at MOI 750 vp/cell and MOI 1500 vp/cell at 24 h and 72 h infection (Figures 4G and J). The total protein content of A549-derived EVs was quantified at both time-points after virus administration. Compared to control vesicles, protein levels in EVs at MOI 300 vp/cell ($P \leq 0.01$), MOI 750 vp/cell ($P \leq 0.0001$), and MOI 1500 vp/cell ($P \leq 0.0001$) showed a significant increase at a 24 h time-point (Figure 4H). Also, we observed that protein levels in EVs at MOI 300 vp/cell were sustainably higher compared to EVs at MOI 1500 vp/cell ($P \leq 0.0001$) after HAdV-5 at 24 h (Figure 4H). Moreover, at MOI 750 vp/cell and MOI 1500 vp/cell EV proteins were elevated significantly post-virus exposure ($P \leq 0.001$; Figure 4H). Similarly, at 72 h HAdV-5 infection, the total protein content values of control vesicles were significantly higher compared to EVs at MOI 1500 vp/cell ($P \leq 0.05$; Figure 4K). In addition, EV total protein was significantly increased between EVs at MOI 750 vp/cell and vesicles at MOI 1500 vp/cell 72 hpi ($P \leq 0.05$; Figure 4K). Taken together, our results revealed that the vesicles isolated from the media of uninfected A549 cells and HAdV-5 infected A549 cells showed characteristics of small EVs (i.e., exosomes) with regards to their morphology, size, and surface charge thus indicating the successful harvest of exosomes. Meanwhile, this data demonstrated that HAdV-5 significantly elevated the total RNA and protein content within our EVs [2, 25, 27, 28, 49, 50].

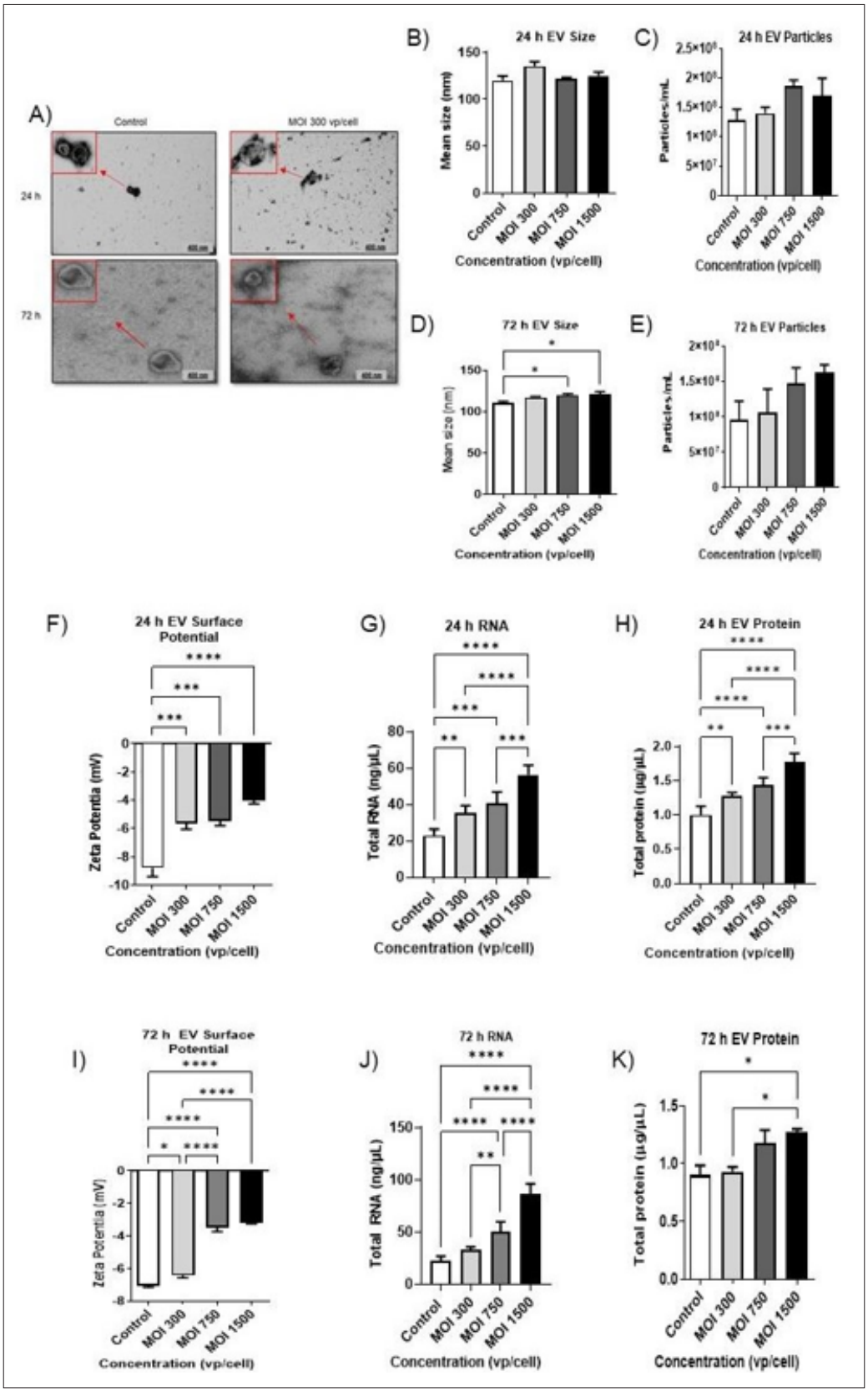


**Figure 4:** Characterization of A549-Derived Vesicles
(A) Morphology of control exosomes and HAdV-5 MOI 300-derived exosomes at 24 h and 72 h; (15,000X magnification) 400 nm scale. (B, D) Zeta view analysis of exosomes mean size and (C, E) concentration following 24 h and 72 h HAdV-5 infection. (F, I) Exosome surface potential at 24 h and 72 h post-virus infection. (G, J) Total RNA of A549-derived EVs at 24 h and 72 h post-HAdV-5 exposure. (H, K) Total protein content of A549-derived EVs at 24 h and 72 h post-virus infection. Statistical significance was obtained from five independent experiments and determined using one-way ANOVA with post hoc Tukey's analysis. Data are presented as the mean ± SEM as follows: (*) $P \leq 0.05$, (**) $P \leq 0.01$, (***) $P \leq 0.001$, and (****) $P \leq 0.0001$.

**Identification of EV-Associated Proteins in HAdV-5-Infected A549-Derived EVs**. EVs were isolated from the media of non-infected and HAdV-5-infected A549 cells using a combination of EV isolation methods, previously described. Western or dot blot analysis was performed to examine the expression of various exosome-associated proteins in EVs after administration of HAdV-5 at 24 h or 72 h (Figures 5 A-D). The expression of Hsp 70 and TLR 6 was evaluated in western blot and dot blot at 72 h virus infection (Figure 5A). Hsp 70 expression levels were slightly elevated in EVs 72 hpi via dot blot analysis (Figure 5A). TLR 6 levels of expression within small EVs were significantly higher among all HAdV-5-infected EV experimental groups (MOI 300, MOI 750, and MOI 1500 vp/cell) compared to the control group ($P \leq 0.05$ and $P \leq 0.01$; Figure 5A). In Figure 5B, we observed a significant increase of Hsp 27 in control EVs and EVs at the highest virus concentration (MOI 1500 vp/cell) ($P \leq 0.001$), EVs at the lowest virus concentration (MOI 300 vp/cell) and MOI 1500 vp/cell ($P \leq 0.01$), and EVs at MOI 750 vp/cell and MOI 1500 vp/cell ($P \leq 0.01$) after 24 h virus exposure. At 72 h, Hsp 27 proteins were expressed among all EVs after HAdV-5 infection (Figure 5B). In Figure 5C, we evaluated the exosome biogenesis marker Rab 35. We found a significant increase in Rab 35 expression levels in EVs at MOI 300 vp/cell and MOI 750 vp/cell HAdV-5 administration at 24 h ($P \leq 0.05$; Figure 5C). At 72 h HAdV-5 exposure, EVs from A549 cells infected with HAdV-5 exhibited a slight increase in all EVs (Figure 5C). To investigate the pro-inflammatory response in EVs obtained from the media of A549 cells after virus infection, we demonstrated the presence of IL-12 (Figure 5D). IL-12 is a cytokine that plays a vital role in the development of cellular immunity. IL-12 activates the immune system by promoting the activation and/or inhibition of cell proliferation. In A549-derived EVs, IL-12 was significantly decreased at the highest HAdV-5 concentration (MOI 1500 vp/cell) when compared to control vesicles at 24 hpi ($P \leq 0.05$; Figure 5D). Similarly, at 72 h virus administration, IL-12 was decreased significantly at MOI 300 vp/cell and MOI 750 vp/cell when compared to the control EVs ($P \leq 0.01$ and $P \leq 0.05$; Figure 5D). This data significantly demonstrated the presence of exosome-associated proteins related to vesicle formation, membrane trafficking, and composition after adenovirus infection. In addition, this data shows that EVs act as carriers for cytokines in response to virus infection.

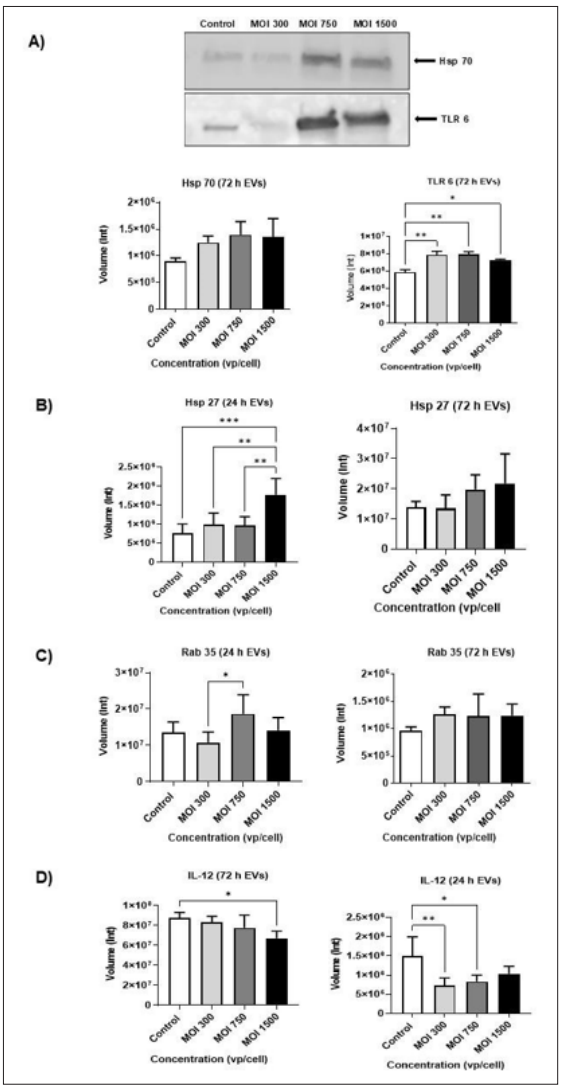


**Figure 5:** Expression of Exosome-Associated Proteins/Markers After HAdV-5 Infection
Western blot and dot blot analysis of A549-derived EVs expressing (A) Hsp 70 and TLR 6 at 72 h HAdV-5 exposure. Exosome proteins were evaluated at 24 h and 72 h post-virus infection via dot blot analysis (B - D). (B) Exosomes were evaluated for Hsp 27 expression. (C) Exosome proteins were evaluated for the expression of exosome biogenesis marker Rab 35. (D) Exosomes were evaluated for interleukin (IL) 12. Statistical significance was obtained from five independent experiments and determined using one-way ANOVA with post hoc Tukey's analysis. Data are presented as the mean ± SEM as follows: (*) $P \leq 0.05$, (**) $P \leq 0.01$, and (***) $P \leq 0.001$.

**Apoptotic Bodies Characterization**

Many types of cells (e.g., epithelial cells, microglial, etc.) in the human body undergo apoptosis, a form of programmed cell death [24, 51]. Cells can undergo apoptosis when triggered by stimuli, such as hypoxia, drugs, pathogens, etc [52]. Specifically, cells can undergo apoptosis in response to viral infection, which decreases the release of progeny virus. It has been reported that viruses modulate host cell apoptosis [53-55]. These viruses may interfere with the highly conserved effector mechanisms of apoptosis or by the regulatory mechanisms specific to–host cells [53, 54]. Apoptosis is characterized by a series of steps that results in cell shrinkage, DNA fragmentation, membrane blebbing, and the formation of ApoBDs. ApoBDs are the largest type of EVs (~ 500 - 2,000 nm). They contain proteins, lipids, microRNA, DNA molecules, chromatins, portions of the cytosol, and intact organelles. Many studies describe the formation of ApoBDs, but little is known about their role in intracellular pathological mechanisms [51, 56-58]. In this study, we investigated the impact of HAdV-5 on large EVs harvested from A549 cells. A549 cells were subjected to HAdV-5 at varying MOIs for the indicated time points, as previously described. ApoBDs were isolated from the conditioned media of either non-infected or infected A549 cells using low and high speed centrifugation, and filtration. ApoBDs are large vesicles generated by cells undergoing apoptosis [51]. Detection and characterization of large EVs (i.e. ApoBDs) were observed by SEM, zeta size, and zeta potential. Figure 6A shows SEM imaging analysis of vesicles collected from cell culture media of A549 cells. SEM data revealed the presence of large spherical vesicles with a size of 1,000 - 5,000 nm at the 72 h time-point. Zeta size analysis showed that our large EVs were < 1000 nm in size at both 24 h and 72 h time-points after HAdV-5 administration (Figures 6B and C). Zeta potential distribution showed that the vesicles contained a net negative surface charge and exhibited a zeta potential range of -7.12 to -9.37 mV after 24 h and 72 h HAdV-5 administration (Figures 6D and E). At 24 hpi, the surface potential of the vesicles was significantly reduced in all infectious groups compared to the control group ($P \leq 0.05$ and $P \leq 0.01$; Figure 6D). At 72 h, the zeta potential was significantly unchanged between control EVs and infection EVs after HAdV-5 exposure (Figure 6D). Total EV protein levels were evaluated within our samples after the desired infection time (Figure 6F and G). At 24 h, the protein content of large vesicles was significantly lowered at the lowest virus concentration when compared to non-infected vesicles ($P \leq 0.05$; Figure 6F). However, at 72 h, we demonstrated a significant increase in total protein in ApoBDs at MOI 750 vp/cell and MOI 1500 vp/cell ($P \leq 0.01$; Figure 6G). Thus, our results showed that HAdV-5 did not significantly impact the mean size of ApoBDs harvested from the media of A549 cells. However, this data indicates that HAdV-5 has a significant impact on the surface potential, as well as total protein concentration in our ApoBDs in a dose-dependent manner and at relative time points. More analysis is needed to highlight the specific contributions of ApoBDs involvement in intercellular communications and human health and diseases.

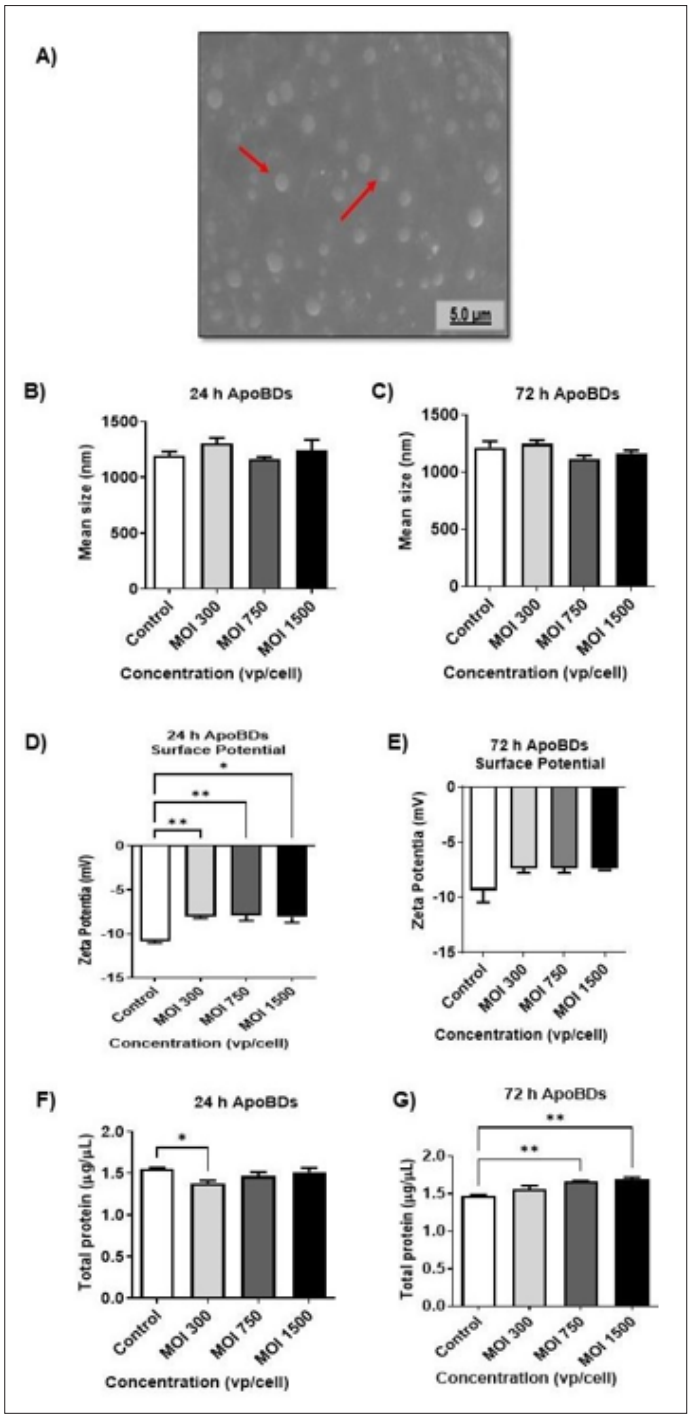


**Figure 6:** A549-Derived Apoptotic Bodies Characterization (A) Scanning electron microscopy of control ApoBDs at 72 h; (1500 X magnification) 5.0 µm scale. Arrows indicated the presence of vesicles. (B-C) Zetaview analysis of ApoBDs` mean size at 24 h and 72 h post HAdV-5 infection. (D-E) Zeta potential distribution of ApoBDs at 24 h and 72 h after virus administration. (F-G) Total ApoBDs protein quantitation at 24 h and 72 h HAdV-5 infection. Statistical significance: Defined as follows: (*) $P \leq 0.05$, (**) $P \leq 0.01$.

## Discussion

Infectious diseases are among the biggest threats to the general public health. With increased human activity, more viruses have been shown to spread, emerge, remerge, and regulate many cellular mechanisms. Viruses can use EVs to initiate immune evasion and/or facilitate virus spread. This can prompt the development of human infectious diseases, such as HAdV. HAdVs are complex and evolving microorganisms associated with respiratory and gastrointestinal illnesses [1, 2]. Much is already known about the pathogenicity of HAdV. However, a better understanding is needed to prevent the infectivity and spread of these viruses. New information about the interactions between HAdVs and EVs may help to describe viral entry paradigms. Clarifying these mechanisms may lead to better diagnostics and the development of innovative therapeutic modalities against various common and emerging viral infections. This study contributes to understanding the impact of HAdV-5 on the physiochemical properties (size, concentration, and charge) and cargo composition of lung cancer cells and lung cancer-derived EVs. We illustrated that HAdV-5 modulates the cellular biogenesis of A549 cells. Our findings showed that HAdV-5 infection resulted in substantial changes in the number of viable cells at all virus concentrations after post-virus administration compared to control cells ($P \leq 0.05$ and $P \leq 0.0001$; Figure 1B and C). Our data indicate that HAdV-5 causes cell death in human lung carcinoma cells. These observations were further confirmed by fluorescence microscopy, MTT assay, and stress-response to hsps and apoptotic regular proteins via dot blot analysis.

This study aims to further examine the role of small EVs (i.e., exosomes) and large EVs (i.e., ApoBDs) in virus progression by evaluating the effect of HAdV-5 exposure on the production and composition of EVs in vitro. Virus infections can cause EV formation and secretion from infected host cells. EVs purified from culture supernatants of HAdV-5-infected A549 cells were characterized using our standard methods [2, 28, 59]. Microscopic analysis revealed that HAdV-5 infection stimulated the release of multiple EV subpopulations. These vesicles resembled small EVs (i.e., exosomes) (~50 nm-150 nm) and large EVs (i.e., ApoBDs) (~1,000 nm- 5,00nm), which were similar to morphological features of vesicles previously reported [2, 28, 59-61]. Furthermore, the total number of exosomes (particles/mL) produced slightly increased at MOI 1500 of HAdV-5 administration compared with the control exosomes. In a previous study by our group, we observed contrasting effects on EV production after HAdV-3 treatment. We noticed that the total number of small EVs derived from HAdV-infected cells was reduced compared to non-infected vesicles derived from A549 cells [2]. We observed that the total RNA (Figures 4G and J) and protein (Figures 4H and K) levels of EVs were significantly increased over time after HAdV-5 infection. This could possibly explain the increase in the production of EV particles after virus infection. The ZP of EVs derived from body fluids and conditioned cultures are significantly altered as they interact with various cellular targets [62, 63]. These parameters reflect the origin and the endocytotic pathway the small EVs (i.e., exosomes) may utilize. In addition, they are integral-computing properties of cell signaling [63]. Under physiological conditions, EVs carry a net negative surface charge that can contribute to EVs: EV interaction and their cellular uptake by target cells. Our ZP measurements show that both small EVs and large EVs harvested from the cell culture medium of A549 cells possessed a negative charge. The vesicles' ZP measurements were distributed within the range of -6 mV to -40 mV (Figures 4F and I), which correlates with measurements from previously reported literature [49]. EVs with ZP values between -30 mV and +30 mV could agglomerate. Similarly, if the particles have low ZP values (e.g., particles near zero), there will be no electrostatic repulsion between the particles. Therefore, it will cause the particles to aggregate and the suspension will be unstable. However, the exact threshold of stability may vary according to the type of particle [62]. Our study illustrated that HAdV-5 altered the stability of EVs derived from A549 cells. We observed a significant change in the ZP of A549-derived EVs suspended in MilliQue water. A comparison of the zeta potentials at all MOIs indicates that the ZP value of A549-derived EVs was significantly less negative than that of control A549-derived EVs in our ZP measurements after HAdV-5 infection (Figures 4F and I). This trend suggests that at a higher virus concentration, the presence of EVs in a solution can cause repulsion due to HAdV-5 infection, which could indicate aggregation and instability. The effects of human infectious diseases on the ZP of EVs are unfortunately not described enough despite their essential role in stability, pharmacokinetics, and release mechanisms. More research is needed to investigate the ZP of EVs under pathogenic conditions.

EVs carry out a wide range of bodily functions and their cargo is equally varied. Therefore, the specific protein content of EVs may vary within the host species, cellular origin, biofluid, and disease state. Dot blot analysis revealed the presence of proteins associated with lysates and/or exosomes. Here, we observed that HAdV-5 infection led to a significant increase and decrease of various stress response markers in cell lysates ($P \leq 0.05$, $P \leq 0.01$, $P \leq 0.001$, and $P \leq 0.0001$; Figures 2A-E). These proteins are altered in cell lysates after HAdV-5 treatment because they may elicit a pro- or anti- inflammatory response. We examined the expression levels of EV-associated markers CD 63 and actin (data not shown). CD 63 interacts with other membrane receptors and signaling molecules. It plays a role in EV biogenesis, sorting cargo components such as proteins and miRNAs into EVs, and the binding and uptake of EVs by target cells. In the current study, we detected a significant amount of tetraspanin CD 63 in small EVs derived from the culture supernatants at MOI 300 HAdV-infected cells compared to uninfected cells ($P \leq 0.05$) (data not shown). Actin is a cytoskeletal EV-associated protein. Actin is a key component of the cellular cytoskeleton that facilitates AdV intracellular translocation to the nucleus. We found that actin is highly enriched in A549-derived EVs after virus infection ($P \leq 0.05$ and $P \leq 0.01$) (data not shown). Viruses (i.e., AdV and coronavirus) use the actin cytoskeleton for entry, assembly, and egress from the host cell [64]. Viruses hijack many actin functions and alter or redirect them to augment self-propagation [66]. Hsp 27 is a member of the small HSP protein family and is involved in a variety of biological activities. Hsp 27 plays a key role in supporting cell survival under virus-related stress conditions. Our laboratory demonstrated that the levels of HSP27 significantly increased in EVs among all experimental groups post-HAdV-5 infection ($P \leq 0.01$ and $P \leq 0.001$; Figure 5B). Several studies that have reported the role of Hsp27 in different viruses indicating its role as both a pro-viral and antiviral factor through various mechanisms involving different signaling pathways [39, 67]. In a 2019 study by Dan et al, the group demonstrated that Hsp27 plays a key role in regulating the human pathogen Enterovirus 71. They showed that Hsp 27 supports EV-A71 infection to promote viral internal ribosome entry site-dependent translation [68]. Hsp 70 is a classical exosome marker. Hsp 70 interacts with viral polymerase to augment viral replication. They can facilitate the development of a viral replication complex and/or maintain the stability of complex proteins [69]. We detected Hsp 70 in our EV samples at

a 72 h time-point via western blot and dot blot analysis (Figure 5A). We observed increasing levels of Hsp 70 expression in control vesicles, as well as vesicles at 72 h HAdV-5 infection (Figure 5A). We also evaluated Rab 35, an exosome biogenesis marker. Rab 35 is a GTPase protein involved in membrane trafficking,vesicle formation, and secretion [70]. The endosome-associate protein was detected in exosomes produced by non-infected and HAdV-5-infected A549 cells in a dose-dependent manner ($P \leq 0.05$; Figure 5C). These observations illustrate that the membrane components of vesicles resemble those of exosomes.

The immune system uses toll-like receptors to recognize pathogenic foreign nucleic acid [71]. TLRs bind to viral dsRNA and ssRNA, as well as viral DNA. TLRs of various cell types (e.g., epithelial cells) activate cells when they come into contact with exosomes containing viral miRNA [72, 73]. It has been demonstrated that AdV infection induces a multi-faceted innate cellular immune response facilitated by the TLR pathway in A549 epithelial cells [74, 75]. With this information, we examined immunomodulatory proteins TLR3 (data not shown), TLR6, and IL-12. TLR3 and TLR 6 are type I transmembrane glycoprotein receptors that recognize microbial pathogens (e.g., bacteria and viruses) and activate the innate immune response. They recognize distinct pathogen-associate molecular patterns and damage-associate molecular patterns expressed on infectious agents. In addition, they mediate the production of cytokines necessary to develop adequate immunity [72]. Chen et al. reported that plasma exosomes purified from COVID-19 patients containing SARS-CoV-2, a single-stranded RNA-enveloped virus, significantly increased the expression of TLR. In contrast, we observed that EVs isolated from HAdV-5-infected cells showed significantly lower levels of TLR 3 expression ($P \leq 0.05$ and $P \leq 0.01$) (data not shown). This shows a reduction in TLR3 expression levels in EVs because it is not abundant in dsDNA viruses, such as HAdV. TLR6 expression was identified in EVs through western blot at a 72 h time- point (Figure 5A). Through dot analysis, we observed that TLR 6 significantly elevated in EVs at all MOIs compared with control at 72 h HAdV-5 administration ($P \leq 0.05$ and $P \leq 0.01$; Figure 5A). IL- 12 is known to initiate pro-inflammatory cytokines in epithelial cells. Our study confirms these findings. We observed a significant reduction in IL-12 expression in our EVs at the relative time points after HAdV- 5 infection ($P \leq 0.05$ and $P \leq 0.01$; Figure 5D). This data suggests that exosomes may modulate various pro-inflammatory immune responses during HAdV-5 infection in vitro. Apoptosis is a form of programmed cell death. In virus-infected cells, apoptosis can be triggered by the cell's intrinsic or extrinsic pathways [53, 55, 76]. The intrinsic (mitochondrial) pathway is activated by intracellular stresses (e.g., DNA damage) and regulated by the Bcl-2 family proteins [77]. The extrinsic pathway is induced by external death signals and caspase activation and mediated by death receptors (e.g., Fas, tumor necrosis factor, etc.). Viruses utilize EVs as an alternative mechanism during host defense in response to infection to inhibit spread and replication [78-80]. The formation of large EVs or ApoBDs occurs during plasma membrane blebbing when cells undergo apoptosis [81, 82]. Information regarding their role in various physiologic and pathologic processes in human infectious diseases is very limited. Identifying and measuring the distribution of intracellular contents (RNA, DNA, and mitochondria) within ApoBDs is complicated. The study of large EVs is challenging due to limited information regarding ApoBD-associated markers and the function of ApoBDs in various disease settings. Our study briefly examines large vesicles isolated from the cell culture medium of lung carcinoma cells infected with HAdV-5. Through electron microscopy, we observed the presence of large spherical vesicles that displayed ApoBD morphological characteristics (Figure 6A). HAdV-5 has no significant impact on the size distribution at the relative time points (Figures 6B and C). Meanwhile, the zeta potential of large vesicles derived from A549 cells as the virus concentrations increased significantly compared to control EVs 24 hpi ($P \leq 0.05$ and $P \leq 0.01$; Figure 6D). Whereas, at 72 h virus administration, no significant change was observed in ApoBDs samples (Figure 6E). This effect on large EVs may be attributed to the viruses' ability to produce their progeny in infected cells. HAdV-5 significantly modulated the total protein content in the large vesicles in a dose- dependent manner at 24 h and 72 hpi ($P \leq 0.05$ and $P \leq 0.01$; Figures 6F and G). More in-depth studies are needed to better understand ApoBDs' role and function under physiological and pathological conditions. This study serves as a good in vitro model for investigating host-pathogen interactions and possibly highlighting the role of EVs in HAdV infection.

## Statements and Declarations

### Acknowledgments
We would like to acknowledge the Center for NanoBiotechnology Research who provided SEM at Alabama State University, Montgomery, AL and the High-Resolution Imaging Facility Service Center who provided TEM at the University of Alabama at Birmingham, Birmingham, AL. Moreover, we would like to acknowledge our funding sources: the Alabama EPSCoR Graduate Research Scholars Program (grant number IOS-1900377) and the Centers for Disease Control and Prevention (grant number: NU38OT000279).

### Funding
This work was supported by the Alabama EPSCoR Graduate Research Scholars Program, grant number IOS-1900377 and B.C. has received research support from the National Science Foundation". Centers for Disease Control and Prevention, grant number is: NU38OT000279.

### Competing Interests
The authors have no relevant financial or non-financial interests to disclose.

### Author Contributions
All authors contributed to the study's conception and design. Material preparation, data collection, and analysis were performed by Qiana L. Matthews, Brennetta J. Crenshaw, Sameer Joshi, Ayodeji O. Ipinmoroti, Rachana Pandit, and Brian Sims. The first draft of the manuscript was written by Brennetta J. Crenshaw and all authors commented on previous versions of the manuscript. All authors read and approved the final manuscript.

### Data Availability
The datasets generated during and/or analyzed during the current are available from the corresponding author upon reasonable request.

### Ethics approval
This is an observational study. The Alabama State University Research Ethnics Committee has confirmed that no ethnical approval is required.

### Consent to Participate
"Not applicable"

### Consent to Publish
"Not applicable"

**References**

1. Crenshaw BJ, Jones LB, Bell CR, Sanjay Kumar, Matthews QL (2019) Perspective on Adenoviruses: Epidemiology, Pathogenicity, and Gene Therapy. Biomedicines 7: 61.
2. Ipinmoroti AO, Crenshaw BJ, Rachana Pandit, Sanjay Kumar, Brian Sims (2021) Human Adenovirus Serotype 3 Infection Modulates the Biogenesis and Composition of Lung Cell-Derived Extracellular Vesicles. J Immunol Res 2021: 2958394.
3. Centers for Disease Control and Prevention (2020) Adenovirus Vaccine Information Sheet. https://www.cdc.gov/vaccines/hcp/vis/vis-statements/adenovirus.html.
4. Greber UF (2020) Adenoviruses - Infection, pathogenesis and therapy. FEBS Letters 594: 1818-1827.
5. Cheong XK, Lau CL, Loong LS, Tajuruddin FW, Periyasamy P, et al. (2020) Fatal adenovirus meningoencephalitis in end stage renal disease patient. International Journal of Infectious Diseases 101: 166-167.
6. Vinters HV, Zhang XR (2020) Adenovirus Meningoencephalitis. Infections of the Central Nervous System: Pathology and Genetics 77-82.
7. Kumar NM (2020) Microbial Conjunctivitis in Principles and practices of infectious diseases. 1497- 1507.
8. Shieh WJ (2022) Human adenovirus infections in pediatric population - An update on clinico–pathologic correlation. Biomedical Journal 45: 38-49.
9. De Francesco MA, Giovanni Lorenzin, Antonella Meini, Richard Fabian Schumacher, Arnaldo Caruso, et al. (2021) Nonenteric Adenoviruses Associated with Gastroenteritis in Hospitalized Children. Microbiology Spectrum 9: e00300-21.
10. Lee B, Damon CF, Platts-Mills JA (2020) Pediatric acute gastroenteritis associated with adenovirus 40/41 in low-income and middle-income countries. Current Opinion in Infectious Diseases 33: 398-403.
11. Stasiak AC, Stehle T (2020) Human adenovirus binding to host cell receptors: a structural view. Medical Microbiology and Immunology 209: 325-333.
12. Schwartze Jt, Havenga M, Bakker Wam, Bradshaw Ac, Nicklin Sa (2022) Adenoviral vectors for cardiovascular gene therapy applications: a clinical and industry perspective. Journal of Molecular Medicine 100: 875-901.
13. Mendonça SA, Lorincz R, Boucher P, David TC (2021) Adenoviral vector vaccine platforms in the SARS-CoV-2 pandemic. npj Vaccines 6: 97.
14. Chang J (2021) Adenovirus Vectors: Excellent Tools for Vaccine Development. Immune Netw 21: e6.
15. Medina GN, de los Santos T, Díaz San Segundo F (2022) Generation of Replication Deficient Human Adenovirus 5 (Ad5) Vectored FMD Vaccines. Methods in Molecular Biology. Clifton N.J 2465: 155-175.
16. Travieso T, Li J, Mahesh S, Juliana Da Fonzeca Redenze E Mello, Blasi M (2022) The use of viral vectors in vaccine development. npj Vaccines 7: 75.
17. Gao J, Mese K, Bunz O, Ehrhardt A (2019) State-of-the-art human adenovirus vectorology for therapeutic approaches. FEBS Letters 593: 3609-3622.
18. Maginnis MS (2018) Virus-Receptor Interactions: The Key to Cellular Invasion. J Mol Biol 430: 2590- 2611.
19. Llorente García I, Marsh M (2020) A biophysical perspective on receptor-mediated virus entry with a focus on HIV. Biochimica et Biophysica Acta (BBA) - Biomembranes 1862: 183158.
20. Boulant S, Stanifer M, Lozach PY (2015) Dynamics of Virus-Receptor Interactions in Virus Binding, Signaling, and Endocytosis. Viruses 7: 2794-2815.
21. Sims B, Gu L, Krendelchtchikov L, Matthews QL (2014) Neural stem cell-derived exosomes mediate viral entry. Int J Nanomedicine 9: 4893-4897.
22. Sims B, Farrow AL, Williams SD, Bansal A, Krendelchtchikov A, et al. (2017) Role of TIM-4 in exosome-dependent entry of HIV-1 into human immune cells. Int J Nanomedicine 12: 4823-4833.
23. Sims B, Farrow AL, Williams SD, Bansal A, Krendelchtchikov A, et al. (2018) Tetraspanin blockage reduces exosome-mediated HIV-1 entry. Arch Virol 163: 1683- 1689.
24. Crenshaw BJ, Kumar S, Bell CR, Jones LB, Williams SD, et al. (2019) Alcohol Modulates the Biogenesis and Composition of Microglia-Derived Exosomes. Biology (Basel) 8: 25.
25. Jones LB, Kumar S, Curry AJ, Price JS, Krendelchtchikov A, et al. (2019) Alcohol Exposure Impacts the Composition of HeLa-Derived Extracellular Vesicles. Biomedicines 7: 78.
26. Bell C, Jones LB, Crenshaw BJ, Kumar S, Rowe GC, et al. (2019) The Role of Lipopolysaccharide-Induced Extracellular Vesicles in Cardiac Cell Death. Biology 8: 69.
27. Jones LB, Kumar S, Bell C, Crenshaw BJ, Coats MT, et al. (2021) Lipopolysaccharide Administration Alters Extracellular Vesicles in Cell Lines and Mice. Curr Microbiol 78: 920-931.
28. Kumar S, Crenshaw BJ, Williams SD, Bell C, Matthews QL, et al. (2021) Cocaine-Specific Effects on Exosome Biogenesis in Microglial Cells. Neurochemical Research 46: 1006-1018.
29. Rimmer MP, Gregory CD, Mitchell RT (2021) The transformative impact of extracellular vesicles on developing sperm. Reproduction and Fertility 2: R51-R66.
30. Neyroud AS, Chiechio R, Yefimova M, Lo Faro MJ, Dejucq Rainsford N, et al. (2021) Extra-cellular vesicles of the male genital tract: new actors in male fertility? Basic and Clinical Andrology 31: 25.
31. Hinzman CP, Jayatilake M, Bansal S, Fish BL, Li Y, et al. (2022) An optimized method for the isolation of urinary extracellular vesicles for molecular phenotyping: detection of biomarkers for radiation exposure. Journal of Translational Medicine 20: 199.
32. Cricrì G, Bellucci L, Montini G, Collino F (2021) Urinary Extracellular Vesicles: Uncovering the Basis of the Pathological Processes in Kidney-Related Diseases. Int J Mol Sci 22: 6507.
33. Jiang X, You L, Zhang Z, Cui X, Zhong H, et al. (2021) Biological Properties of Milk-Derived Extracellular Vesicles and Their Physiological Functions in Infant. Frontiers in Cell and Developmental Biology 9: 693534.
34. O'Reilly D, Dorodnykh D, Avdeenko NV, Nekliudov NA, Garssen J, et al. (2020) Perspective: The Role of Human Breast-Milk Extracellular Vesicles in Child Health and Disease. Advances in Nutrition 12: 59-70.
35. Ipinmoroti AO, Matthews QL (2020) Extracellular Vesicles: Roles in Human Viral Infections, Immune- Diagnostic, and Therapeutic Applications. Pathogens 9: 1056.
36. Troyer Z, Tilton JC (2021) Extracellular vesicles as carriers of viruses. ExRNA 3: 13.
37. Purvinsh L, Gorshkov A, Brodskaia A, Vasin A (2021) Extracellular Vesicles in Viral Pathogenesis: A Case of Dr. Jekyll and Mr. Hyde. Life (Basel) 11: 45.
38. Invitrogen, TRIzol™ (2023) Reagent User Guide. ThermoFisher Scientific. MAN0001271: m1-4. https://assets.thermofisher.com/TFS-Assets/LSG/manuals/trizol_reagent.pdf.
39. Wan Q (2020) Stress proteins: the biological functions in virus

infection, present and challenges for target-based antiviral drug development. Signal Transduction and Targeted Therapy 5: 125.
40. Maleki F, Khosravi A, Nasser A, Taghinejad H, Azizian M, et al. (2016) Bacterial Heat Shock Protein Activity. J Clin Diagn Res 10: BE01–BE03.
41. Obuchowski I, Karaś P, Liberek K (2021) The Small Ones Matter-sHsps in the Bacterial Chaperone Network. Frontiers in Molecular Biosciences 8: 666893.
42. Zhang X, Yu W (2022) Heat shock proteins and viral infection. Frontiers in Immunology 13: 947789.
43. Polster BM, Pevsner J, Hardwick JM (2004) Viral Bcl-2 homologs and their role in virus replication and associated diseases. Biochimica et Biophysica Acta 1644: 211-227.
44. Kvansakul M, Caria S, Hinds MG (2017) the Bcl-2 Family in Host-Virus Interactions. Viruses 9: 290.
45. Yang L, Chen S, Zhao Q, Pan C, Peng L, et al. (2022) Histone deacetylase 3 contributes to the antiviral innate immunity of macrophages by interacting with FOXK1 to regulate STAT1/2 transcription. Cell Rep 38: 110302.
46. Tang JL, Yang Q, Xu CH, Zhao H, Liu YL, et al. (2021) Histone deacetylase 3 promotes innate antiviral immunity through deacetylation of TBK1. Protein Cell 12: 261-278.
47. Wu Y, Deng W, Klinke DJ (2015) Exosomes: improved methods to characterize their morphology, RNA content, and surface protein biomarkers. Analyst 140: 6631-6642.
48. Rikkert LG, Nieuwland R, Terstappen LWMM, Coumans FAW (2019) Quality of extracellular vesicle images by transmission electron microscopy is operator and protocol dependent. J Extracell Vesicles 8: 1555419.
49. Midekessa G, Godakumara K, Ord J, Viil J, Lättekivi F, et al. (2020) Zeta Potential of Extracellular Vesicles: Toward Understanding the Attributes that Determine Colloidal Stability. ACS omega 5: 16701-16710.
50. Beit-Yannai E, Tabak S, Stamer WD (2018) Physical exosome:exosome interactions. Journal of cellular and molecular medicine 22: 2001-2006.
51. Battistelli M, Falcieri E (2020) Apoptotic Bodies: Particular Extracellular Vesicles Involved in Intercellular Communication. Biology 9: 21.
52. Brown DA, Yang N, Ray SD (2014) Apoptosis, in Encyclopedia of Toxicology (Third Edition), P. Wexler, Editor. Academic Press: Oxford 287-294.
53. Rex DAB, Prasad TSK, Kandasamy RK (2022) Revisiting Regulated Cell Death Responses in Viral Infections. International Journal of Molecular Sciences 23: 7023.
54. Kvansakul M (2017) Viral Infection and Apoptosis. Viruses 9: 356.
55. Verburg SG, Lelievre RM, Westerveld MJ, Inkol JM, Sun YL, et al. (2022) Viral-mediated activation and inhibition of programmed cell death. PLoS Pathog 18: e1010718.
56. Santavanond JP, Rutter SF, Atkin-Smith JK, Poon IKH (2021) Apoptotic Bodies: Mechanism of Formation, Isolation and Functional Relevance. Subcell Biochem 97: 61-88.
57. Xu X, Lai Y, Hua ZC (2019) Apoptosis and apoptotic body: disease message and therapeutic target potentials. Bioscience reports 39: BSR20180992.
58. Phan TK, Poon IK, Atkin-Smith GK (2018) Detection and Isolation of Apoptotic Bodies to High Purity. J Vis Exp 58317.
59. Jones LB, Kumar S, Bell CR, Crenshaw BJ, Coats MT, et al. (2021) Lipopolysaccharide administration alters extracellular vesicles in human lung-cancer cells and mice. Curr Microbiol 78: 920-931.
60. Dou G, Tian R, Liu X, Yuan P, Ye Q, et al. (2020) Chimeric apoptotic bodies functionalized with natural membrane and modular delivery system for inflammation modulation. Science Advances 6: eaba2987.
61. Jin Liu, Xinyu Qiu, Yajie Lv, Chenxi Zheng, Yan Dong, et al. (2020) Apoptotic bodies derived from mesenchymal stem cells promote cutaneous wound healing via regulating the functions of macrophages. Stem Cell Research & Therapy 11: 507.
62. Beit-Yannai, E Tabak S, Stamer WD (2018) Physical exosome:exosome interactions. J Cell Mol Med 22: 2001-2006.
63. Rasmussen MK, Pedersen JN, Marie R (2020) Size and surface charge characterization of nanoparticles with a salt gradient. Nature Communications 11: 2337.
64. Fuchsova B, Serebryannyy LA, De Lanerolle P (2015) Nuclear actin and myosins in adenovirus infection. Experimental Cell Research 338: 170-182.
65. Taylor MP, Koyuncu OO, Enquist LW (2011) Subversion of the actin cytoskeleton during viral infection. Nat Rev Microbiol 9: 427-39.
66. Kloc M, Ahmed Uosef, Jarek Wosik, Jacek Z Kubiak, Rafik M Ghobrial (2022) Virus interactions with the actin cytoskeleton-what we know and do not know about SARS-CoV-2. Archives of Virology 167: 737-749.
67. Iyer K, Kailash Chand, Alapani Mitra, Jay Trivedi, Debashis Mitra (2021) Diversity in heat shock protein families: functional implications in virus infection with a comprehensive insight of their role in the HIV-1 life cycle. Cell Stress and Chaperones 26: 743-768.
68. Dan X, Qianya Wan, Lina Yi, Jing Lu, Yang Jiao, et al. (2019) Hsp27 Responds to and Facilitates Enterovirus A71 Replication by Enhancing Viral Internal Ribosome Entry Site-Mediated Translation. J Virol 93: e02322-18.
69. Lubkowska A, Waldemar Pluta, Aleksandra Strońska, Alicja Lalko (2021) Role of Heat Shock Proteins (HSP70 and HSP90) in Viral Infection. Int J Mol Sci 22: 9366.
70. Zhang J, Jiang Z, Shi A (2022) Rab GTPases: The principal players in crafting the regulatory landscape of endosomal trafficking. Computational and Structural Biotechnology Journal 20: 4464-4472.
71. Duan T, Yang Du, Changsheng Xing, Helen Y Wang, Rong-Fu Wang (2022) Toll-Like Receptor Signaling and Its Role in Cell-Mediated Immunity. Front Immunol 13: 812774.
72. El-Zayat SR, Sibaii H, Mannaa FA (2019) Toll-like receptors activation, signaling, and targeting: an overview. Bulletin of the National Research Centre 43: 187.
73. Lester SN, Li K (2014) Toll-like receptors in antiviral innate immunity. J Mol Biol 426: 1246-1264.
74. Hartman ZC, Black EP, Amalfitano A (2007) Adenoviral infection induces a multi-faceted innate cellular immune response that is mediated by the toll-like receptor pathway in A549 cells. Virology 358: 357- 372.
75. Zhu J, Huang X, Yang Y (2007) Innate Immune Response to Adenoviral Vectors Is Mediated by both Toll-Like Receptor-Dependent and -Independent Pathways. Journal of Virology 81: 3170-3180.
76. Fang Y, Peng K (2022) Regulation of innate immune responses by cell death-associated caspases during virus infection. The FEBS Journal 289: 4098-4111.
77. Lossi L (2022) The concept of intrinsic versus extrinsic apoptosis. Biochemical Journal 479: 357-384.
78. Barber GN (2001) Host defense, viruses and apoptosis. Cell Death & Differentiation 8: 113-126.
79. Nainu F, Shiratsuchi A, Nakanishi Y (2017) Induction of Apoptosis and Subsequent Phagocytosis of Virus-Infected Cells as an Antiviral Mechanism. Frontiers in Immunology 8: 1220.

80. Atkin-Smith GK, Mubing Duan, Damien J Zanker, Liyen Loh, Thi H O Nguyen, et al. (2020) Monocyte apoptotic bodies are vehicles for influenza A virus propagation. Communications Biology 3: 223.
80. Caruso S, Poon IKH (2018) Apoptotic Cell-Derived Extracellular Vesicles: More Than Just Debris. Frontiers in Immunology 9: 1486.
81. Phan TK, Ozkocak DC, Poon IKH (2020) Unleashing the therapeutic potential of apoptotic bodies. Biochemical Society Transactions 48: 2079-2088.